

# Broadband Impedance Response Extraction of On-Chip Interdigital Capacitors using a 3-D DSA Operator for Piecewise Homogeneous Structures

Tim Pattyn<sup>1</sup>, Xiao Sun<sup>2</sup>, Eric Beyne<sup>2</sup>, Daniël De Zutter<sup>1</sup>, Martijn Huynen<sup>1</sup> and Dries Vande Ginste<sup>1</sup>  
<sup>1</sup>quest, Department of Information Technology, Ghent University - imec, Belgium  
<sup>2</sup>imec, Belgium

**Abstract**—In this contribution, an enhanced 3-D differential surface admittance operator is proposed, facilitating accurate modeling of piecewise homogeneous cuboidal objects. By exploiting the analytical properties of entire-domain basis functions, material interfaces are effectively eliminated from the formulation, leading to a reduction in the number of unknowns without compromising the accuracy of the operator. After a validation of the novel approach, its effectiveness is demonstrated through the analysis of the impedance responses of on-chip interdigital capacitor structures.

**Index Terms**—3-D differential surface admittance (DSA) operator, single-source boundary integral equation (BIE), piecewise homogeneous media, material interfaces, on-chip capacitor

## I. INTRODUCTION

THE relentless drive for more data, faster processing, and greater connectivity is pushing the boundaries of modern technology. To meet these demands, systems are becoming increasingly compact while operating at ever higher frequencies. This shift toward miniaturization and high-speed performance poses new challenges for signal integrity, making it essential to accurately model every component involved.

However, achieving accurate modeling is often non-trivial due to the inherent heterogeneity of state-of-the-art component, which are often tackled by leveraging volumetric meshing in numerical modeling approaches. Still, boundary integral equation (BIE) methods present a compelling alternative by eliminating the need to discretize the entire volume, as such offering smaller system sizes and potentially a more efficient computation. Nonetheless, traditional BIE formulations often require special attention when dealing with conductive media [1]. A promising solution to this limitation is provided by the differential surface admittance operator (DSA) [2], which enables the replacement of the object's material with the background medium by introducing a fictitious surface current density, while eliminating the dependence on Green's functions within the object's interior as well.

In this contribution, we propose a novel 3-D method based on the DSA operator for the accurate and efficient modeling of piecewise homogeneous cuboidal structures, often found in

This work was supported by the Research Foundation-Flanders (FWO) under Grant 1S04425N.

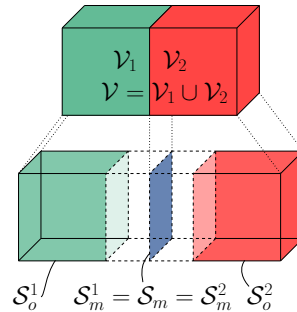


Fig. 1: Piecewise homogeneous cuboid  $\mathcal{V}$  consisting of two homogeneous subregions  $\mathcal{V}_1$  and  $\mathcal{V}_2$ . The surface of  $\mathcal{V}_i$  is called  $\mathcal{S}^i = \mathcal{S}_o^i \cup \mathcal{S}_m$  for  $i = 1, 2$ . The total cuboid  $\mathcal{V}$  has a boundary surface  $\mathcal{S} = \mathcal{S}_o^1 \cup \mathcal{S}_o^2$ .

on-chip interconnects and passive components. Unlike established DSA-based approaches [3], [4], the proposed technique avoids introducing surface current densities at internal material interfaces by eliminating them upfront during the operator construction, resulting in a substantial reduction in the number of unknowns. Furthermore, it maintains compatibility with traditional single-source electric field integral equation (EFIE) formulations.

## II. FORMULATION OF THE METHOD

Consider the piecewise homogeneous cuboid  $\mathcal{V}$ , illustrated in Fig. 1, with its bounding surface defined as  $\mathcal{S} = \mathcal{S}_o^1 \cup \mathcal{S}_o^2$ . The cuboid consists of two homogeneous subregions,  $\mathcal{V}_1$  and  $\mathcal{V}_2$ , whose boundary surfaces are given by  $\mathcal{S}^1 = \mathcal{S}_o^1 \cup \mathcal{S}_m$  and  $\mathcal{S}^2 = \mathcal{S}_o^2 \cup \mathcal{S}_m$ , respectively. Here,  $\mathcal{S}_m$  denotes the internal material interface between the two subregions  $\mathcal{V}_1$  and  $\mathcal{V}_2$ . As mentioned before, our goal is to derive a DSA operator that does not introduce surface current densities on the internal material interface  $\mathcal{S}_m$ .

We start by expanding the tangential electric field and the rotated tangential magnetic field on  $\mathcal{S}_1$  and  $\mathcal{S}_2$  in terms of entire-domain basis functions (EDBFs) [3] to facilitate a discretized representation of the fields. To clearly distinguish the tangential electric field coefficients linked to the inner material interface  $\mathcal{S}_m$  from those related to the remaining cuboid faces  $\mathcal{S}_o^i$  ( $i = 1, 2$ ), we separate them into coefficient vectors  $\bar{\mathbf{e}}^{i,m}$  and  $\bar{\mathbf{e}}^{i,o}$  ( $i = 1, 2$ ), respectively. Applying the

same partitioning to the rotated tangential magnetic field coefficients, allows to link all vectors as follows:

$$\begin{bmatrix} \bar{\mathbf{h}}^{i,o} \\ \bar{\mathbf{h}}^{i,m} \end{bmatrix} = \begin{bmatrix} \bar{\mathcal{P}}^{i,oo} & \bar{\mathcal{P}}^{i,om} \\ \bar{\mathcal{P}}^{i,mo} & \bar{\mathcal{P}}^{i,mm} \end{bmatrix} \begin{bmatrix} \bar{\mathbf{e}}^{i,o} \\ \bar{\mathbf{e}}^{i,m} \end{bmatrix}, (i = 1, 2), \quad (1)$$

where  $\bar{\mathcal{P}}^1$  and  $\bar{\mathcal{P}}^2$  are the discretized Poincaré-Steklov (PS) operators, which map the tangential electric field coefficients onto the rotated tangential magnetic field coefficients, associated with the homogeneous subregions  $\mathcal{V}_1$  and  $\mathcal{V}_2$ , respectively. Each block matrix is labeled with an additional superscript indicating its role.

Continuity of the tangential magnetic field may be imposed on a function-by-function basis, owing to the mutual orthogonality of the EDBFs on  $\mathcal{S}_m$ . Therefore, we get:

$$\begin{aligned} \bar{\mathbf{h}}^{1,m} + \bar{\mathbf{h}}^{2,m} &= \bar{\mathcal{P}}^{1,mm} \bar{\mathbf{e}}^{1,m} + \bar{\mathcal{P}}^{1,mo} \bar{\mathbf{e}}^{1,o} \\ &\quad + \bar{\mathcal{P}}^{2,mm} \bar{\mathbf{e}}^{2,m} + \bar{\mathcal{P}}^{2,mo} \bar{\mathbf{e}}^{2,o} \\ &= 0, \end{aligned} \quad (2)$$

where the plus sign on the left-hand side of (2) is caused by the opposite orientation of the outward-pointing normal vectors on both volumes at  $\mathcal{S}_m$ . By enforcing continuity of the tangential electric field on  $\mathcal{S}_m$ , i.e.,  $\bar{\mathbf{e}}^m = \bar{\mathbf{e}}^{1,m} = \bar{\mathbf{e}}^{2,m}$ , and rearranging the result, we obtain the following expression for  $\bar{\mathbf{e}}^m$ :

$$\bar{\mathbf{e}}^m = -\bar{\mathcal{A}}^{-1} \cdot (\bar{\mathcal{P}}^{1,mo} \bar{\mathbf{e}}^{1,o} + \bar{\mathcal{P}}^{2,mo} \bar{\mathbf{e}}^{2,o}), \quad (3)$$

where  $\bar{\mathcal{A}} = (\bar{\mathcal{P}}^{1,mm} + \bar{\mathcal{P}}^{2,mm})$ . Note that (3) represents  $\bar{\mathbf{e}}^m$  as a linear combination of  $\bar{\mathbf{e}}^{1,o}$  and  $\bar{\mathbf{e}}^{2,o}$ . Hence, the specific choice of EDBFs allows the expansion coefficients of the tangential electric field on the shared interface  $\mathcal{S}_m$  to be directly expressed in terms of those on the outer surfaces  $\mathcal{S}_o^1$  and  $\mathcal{S}_o^2$  of  $\mathcal{V}_1$  and  $\mathcal{V}_2$ , respectively.

As a final step, substituting (3) into (1), and subsequently collecting all the terms, yields the following structure for the discretized PS operator  $\bar{\mathcal{P}}_{\text{tot}}$  associated with the object  $\mathcal{V}$ :

$$\begin{bmatrix} \bar{\mathbf{h}}^{1,o} \\ \bar{\mathbf{h}}^{2,o} \end{bmatrix} = \begin{bmatrix} \bar{\mathcal{P}}_{11} & \bar{\mathcal{P}}_{12} \\ \bar{\mathcal{P}}_{21} & \bar{\mathcal{P}}_{22} \end{bmatrix} \cdot \begin{bmatrix} \bar{\mathbf{e}}^{1,o} \\ \bar{\mathbf{e}}^{2,o} \end{bmatrix} = \bar{\mathcal{P}}_{\text{tot}} \cdot \bar{\mathbf{e}}_{\text{t}} \quad (4)$$

with

$$\bar{\mathcal{P}}_{11} = \bar{\mathcal{P}}^{1,oo} - \bar{\mathcal{P}}^{1,om} \bar{\mathcal{A}}^{-1} \bar{\mathcal{P}}^{1,mo} \quad (5)$$

$$\bar{\mathcal{P}}_{12} = -\bar{\mathcal{P}}^{1,om} \bar{\mathcal{A}}^{-1} \bar{\mathcal{P}}^{2,mo} \quad (6)$$

$$\bar{\mathcal{P}}_{21} = -\bar{\mathcal{P}}^{2,om} \bar{\mathcal{A}}^{-1} \bar{\mathcal{P}}^{1,mo} \quad (7)$$

$$\bar{\mathcal{P}}_{22} = \bar{\mathcal{P}}^{2,oo} - \bar{\mathcal{P}}^{2,om} \bar{\mathcal{A}}^{-1} \bar{\mathcal{P}}^{2,mo} \quad (8)$$

The PS matrix  $\bar{\mathcal{P}}_{\text{tot}}$  is partitioned into four blocks  $\bar{\mathcal{P}}_{ij}$  ( $i, j = 1, 2$ ), where each block maps the tangential electric field expansion coefficients on  $\mathcal{S}_o^j$ , collected in  $\bar{\mathbf{e}}^{j,o}$ , onto the rotated tangential magnetic field expansion coefficients on  $\mathcal{S}_o^i$ , collected in  $\bar{\mathbf{h}}^{i,o}$ . Applying the same procedure to the equivalent configuration, where all materials within  $\mathcal{V}$  are replaced by the background medium, yields the PS matrix  $\bar{\mathcal{P}}_{0,\text{tot}}$ . The

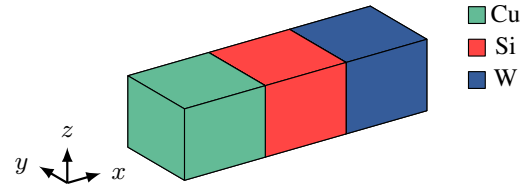


Fig. 2: Composite block consisting of copper ( $\sigma = 5.8 \times 10^7$ ), silicon ( $\epsilon_r = 11.2$ ,  $\sigma = 10$ ) and tungsten ( $\sigma = 1.8 \times 10^7$ ). Each individual segment has dimensions  $30 \text{ mm} \times 30 \text{ mm} \times 30 \text{ mm}$ . resulting DSA operator for  $\mathcal{V}$ , discretized using EDBFs, is subsequently found as:

$$\bar{\mathcal{Y}}_{\text{tot}} = \bar{\mathcal{P}}_{\text{tot}} - \bar{\mathcal{P}}_{0,\text{tot}}. \quad (9)$$

This operator  $\bar{\mathcal{Y}}_{\text{tot}}$  encapsulates all necessary information to determine the expansion coefficients of the surface current density  $\bar{\mathbf{j}}_{\text{s}} = \bar{\mathcal{Y}}_{\text{tot}} \cdot \bar{\mathbf{e}}_{\text{t}}$  on  $\mathcal{S} = \mathcal{S}_o^1 \cup \mathcal{S}_o^2$ , while inherently accounting for the piecewise homogeneous nature of  $\mathcal{V}$ , and without requiring the explicit introduction of a surface current density on the material interface  $\mathcal{S}_m$ .

Following a procedure similar to the one outlined in [3], the newly derived DSA operator is subsequently transformed to local rooftop functions allowing seamless integration with the augmented electric field integral equation [5]. This complete system can now be used for accurate, broadband characterization of heterogeneous on-chip structures.

### III. NUMERICAL EXAMPLES

To validate the proposed approach, we consider the composite block presented in Fig. 2. This block consists of three distinct materials: copper ( $\sigma = 5.8 \times 10^7$ ), silicon ( $\epsilon_r = 11.2$ ,  $\sigma = 10$ ) and tungsten ( $\sigma = 1.8 \times 10^7$ ) with each individual segment having dimensions  $30 \text{ mm} \times 30 \text{ mm} \times 30 \text{ mm}$ . We compare our new method with results obtained from two other solvers: CST Microwave Studio's (CST MWS) frequency-domain solver [6], and the wire method from [3].

A plane wave is propagating in the positive  $y$ -direction with its electric field polarized along the vector  $\bar{\mathbf{p}} = (1, 0, 1)$  at a frequency of 5 GHz. This plane wave is incident on the composite block and the resulting bistatic radar cross-section (RCS) in the  $xy$ -plane, as a function of the azimuth angle  $\phi$ , is provided in Fig. 3. An excellent agreement is observed between our proposed method and CST MWS while the wire method [3] fails to provide an accurate result. This discrepancy is expected, given the presence of silicon in the composite block and the fact that the wire method is only applicable to good conductors ( $\sigma \gg \omega\epsilon$ ), underscoring the need for our novel approach to maintain accuracy. Moreover, our solution only took 33.6 s while consuming 373.8 MB of memory, which is a significant reduction compared to CST MWS's 661s and 9664.9 MB on the same machine.

We now shift our attention to the application examples, i.e., interdigital capacitor structures depicted in Fig. 4. Both configurations represent interdigital capacitors, differing in the number of capacitor elements. Copper ( $\sigma = 5.8 \times 10^7 \text{ S/m}$ ) is used for the metallization, while a high-permittivity dielectric

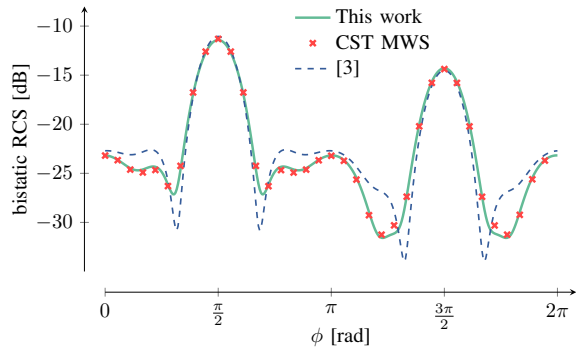


Fig. 3: Bi-static RCS in the  $xy$ -plane of the composite block depicted in Fig. 2. The plane wave is propagating in the positive  $y$ -direction with its electric field polarized along the vector  $\bar{\mathbf{p}} = (1, 0, 1)$  at a frequency of 5 GHz.

material ( $\epsilon_r = 21$ ,  $\tan \delta = 0.01$ ) serves as the inter-metal dielectric. These structures are embedded within a  $\text{SiO}_2$  ( $\epsilon_r = 3.9$ ,  $\tan \delta = 0.001$ ) background, reflecting typical on-chip integration practices. All copper parts have a thickness of  $2 \mu\text{m}$  while the dielectrics have a thickness  $500 \text{ nm}$ . The capacitor has an area of  $50 \mu\text{m} \times 20 \mu\text{m}$ , the signal traces have a width of  $5 \mu\text{m}$ , the vias connecting the top and bottom capacitor plate have a cross section of  $2.5 \mu\text{m} \times 2.5 \mu\text{m}$  and a height of  $3 \mu\text{m}$ . The other relevant dimensions are indicated on Fig. 4 and expressed in  $\mu\text{m}$ .

The impedance response of both structures as a function of frequency is extracted and shown in Fig. 5. To validate the impedance response of both capacitor structures, we included the analytical impedance of an ideal parallel-plate capacitor, a good approximation since the plate area is much larger than the spacing, making stray capacitance negligible. In addition, we included the loop impedance obtained by replacing the dielectric with copper and using the method described in [3]. This enables validation beyond the self-resonance point, where inductive effects dominate. Both additional results confirm the accuracy of our method, demonstrating its suitability for modeling heterogeneous on-chip structures. Moreover, our approach yields a 15% reduction in the number of unknowns compared to established DSA techniques [3], [4], which supports improved computational efficiency, even when considering the limited overhead associated with removing the material interfaces. Notably, CST MWS was unable to produce convincing results for these structures.

#### IV. CONCLUSIONS

In this work, we presented a new DSA operator for piecewise homogeneous cuboidal structures. To this end, analytical properties of entire-domain basis functions were leveraged to effectively remove material interfaces from the simulation domain. This results in a method that is capable of accurately modeling high-contrast material interfaces with a reduced number of unknowns. The results were validated against a state-of-the-art solver and the appositeness was demonstrated by analyzing the broadband impedance response of interdigital on-chip capacitors.

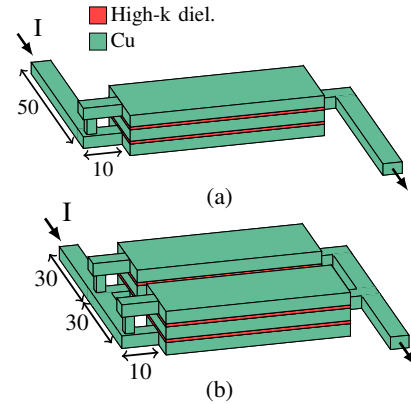


Fig. 4: Interdigital capacitor structures with copper metalization ( $\sigma = 5.8 \times 10^7 \text{ S/m}$ ) and high- $k$  inter-metal dielectric ( $\epsilon_r = 21$ ,  $\tan \delta = 0.01$ ). The capacitor plates have an area of  $50 \mu\text{m} \times 20 \mu\text{m}$ . In (a), a single capacitor element is used, while in (b) two capacitor elements are placed in parallel.

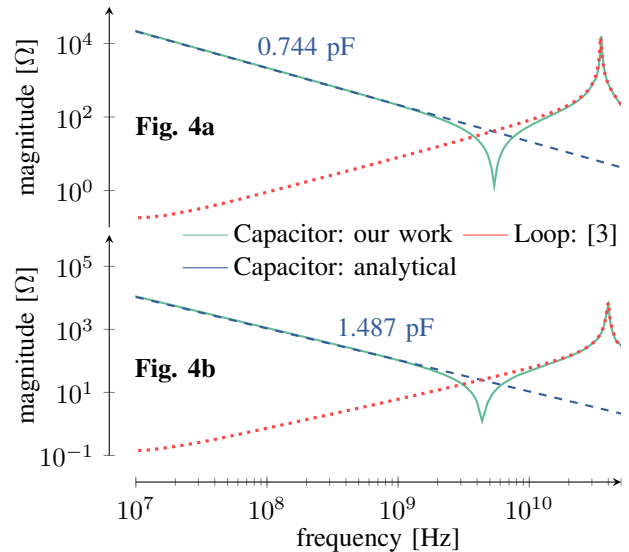


Fig. 5: Impedance response of the interdigital capacitors presented in Fig. 4.

#### REFERENCES

- [1] J. Peeters, I. Bogaert, and D. De Zutter, "Calculation of MoM interaction integrals in highly conductive media," *IEEE Transactions on Antennas and Propagation*, vol. 60, no. 2, pp. 930–940, 2012.
- [2] D. De Zutter and L. Knockaert, "Skin effect modeling based on a differential surface admittance operator," *IEEE Transactions on Microwave Theory and Techniques*, vol. 53, no. 8, pp. 2526–2538, 2005.
- [3] M. Huynen, K. Y. Kapusuz, X. Sun, G. Van der Plas, E. Beyne, D. De Zutter, and D. Vande Ginste, "Entire domain basis function expansion of the differential surface admittance for efficient broadband characterization of lossy interconnects," *IEEE Transactions on Microwave Theory and Techniques*, vol. 68, no. 4, pp. 1217–1233, 2020.
- [4] U. R. Patel, P. Triverio, and S. V. Hum, "A single-source surface integral equation formulation for composite dielectric objects," in *2017 IEEE International Symposium on Antennas and Propagation & USNC/URSI National Radio Science Meeting*, pp. 1453–1454, 2017.
- [5] Z.-G. Qian and W. C. Chew, "Fast full-wave surface integral equation solver for multiscale structure modeling," *IEEE Transactions on Antennas and Propagation*, vol. 57, no. 11, pp. 3594–3601, 2009.
- [6] Dassault Systèmes, *CST Studio Suite*, 2024. <https://www.3ds.com/products-services/simulia/products/cst-studio-suite>.